Published in final edited form as:
Cell Rep. 2012 March 29; 1(3): 200–207.

Assembly and Regulation of the Membrane Attack Complex Based on Structures of C5b6 and sC5b9

Michael A. Hadders[1,7,8], **Doryen Bubeck**[2,7], **Pietro Roversi**[3], **Svetlana Hakobyan**[4], **Federico Forneris**[1], **B. Paul Morgan**[4], **Michael K. Pangburn**[5], **Oscar Llorca**[6,*], **Susan M. Lea**[3,*], and **Piet Gros**[1,*]

[1]Crystal and Structural Chemistry, Bijvoet Center for Biomolecular Research, Department of Chemistry, Faculty of Science, Utrecht University, Padualaan 8, 3584 CH Utrecht, The Netherlands [2]Division of Structural Biology, Wellcome Trust Centre for Human Genetics, University of Oxford, Oxford OX3 7BN, UK [3]Sir William Dunn School of Pathology, University of Oxford, South Parks Road, Oxford OX1 3RE, UK [4]Department of Medical Biochemistry and Immunology, School of Medicine, Cardiff University, Heath Park, Cardiff CF14 4XN, UK [5]Department of Biochemistry, Center for Biomedical Research, University of Texas Science Center, 11937 US Highway 271, Tyler, TX 75708-3154, USA [6]Centro de Investigaciones Biológicas (CIB), Spanish National Research Council (CSIC), Ramiro de Maeztu, 9. 28040 Madrid, Spain

SUMMARY

Activation of the complement system results in formation of membrane attack complexes (MACs), pores that disrupt lipid bilayers and lyse bacteria and other pathogens. Here, we present the crystal structure of the first assembly intermediate, C5b6, together with a cryo-electron microscopy reconstruction of a soluble, regulated form of the pore, sC5b9. Cleavage of C5 to C5b results in marked conformational changes, distinct from those observed in the homologous C3-to-C3b transition. C6 captures this conformation, which is preserved in the larger sC5b9 assembly. Together with antibody labeling, these structures reveal that complement components associate through sideways alignment of the central MAC-perforin (MACPF) domains, resulting in a C5b6-C7-C8β-C8α-C9 arc. Soluble regulatory proteins below the arc indicate a potential dual mechanism in protection from pore formation. These results provide a structural framework for understanding MAC pore formation and regulation, processes important for fighting infections and preventing complement-mediated tissue damage.

[*]Correspondence: ollorca@cib.csic.es (O.L.), susan.lea@path.ox.ac.uk (S.M.L.), p.gros@uu.nl (P.G.) .
[7]These authors contributed equally to this work
[8]Present address: Medical Research Council, Laboratory of Molecular Biology, Hills Road, Cambridge CB2 0QH, UK

ACCESSION NUMBERS Coordinates and structure factors for the crystal structure of C5b6 have been deposited in the Protein Data Bank under accession code 4A5W. The cryo-electron microscopy density map for sC5b9 has been deposited at the Electron Microscopy Data Bank under accession number EMD-1991.

SUPPLEMENTAL INFORMATION Supplemental Information includes four figures, three tables, and one movie and can be found with this article online at doi:10.1016/j.celrep.2012.02.003.

Europe PMC Funders Author Manuscripts

INTRODUCTION

Proteins of the terminal pathway of complement provide immune protection by forming lytic pores, membrane attack complexes (MACs), in membranes (Esser, 1994). Genetic deficiencies of MAC components lead to recurrent infections (Botto et al., 2009); however, unregulated MAC formation causes tissue damage (Morgan, 1999). Formation of the MAC is a sequential process. Upon complement activation, C5 is cleaved into C5a and C5b by the C5 convertase. C6 then captures a labile binding site in C5b (half-life: 2 min) (Cooper and Müller-Eberhard, 1970), followed by C7 association that renders the complex lipophilic (Preissner et al., 1985; Stewart et al., 1987). Binding of heterotrimeric C8αβγ defines the initial membrane insertion event, with C8β mediating attachment to the assembly precursor (Brannen and Sodetz, 2007; Stewart et al., 1987) and C8α penetrating the bilayer (Steckel et al., 1983). Inserted C5b8 functions as a receptor for C9 and catalyzes its oligomerization, leading to membrane perforation and target cell lysis (Podack et al., 1982; Tschopp, 1984; Tschopp et al., 1985). Off-target assembly of the MAC in solution leads to binding of clusterin and vitronectin, yielding a soluble complex called sC5b9 or sMAC. Dissociation of these chaperones by detergents reconstitutes membrane binding (Bhakdi et al., 1979; Podack and Müller-Eberhard, 1980). In addition, sC5b9 and the lytic MAC share a neo-epitope present in C9 that is associated with pore formation (Mollnes et al., 1985), suggesting similarities in how the soluble and membrane-associated complexes are assembled.

MAC proteins and the homologous perforin are proposed to form β-barrel pores on the basis of the structural resemblance between MAC-perforin (MACPF) domains and bacterial cholesterol-dependent cytolysins (CDCs) (Hadders et al., 2007; Law et al., 2010; Lovelace et al., 2011; Rosado et al., 2007; Rossjohn et al., 1997; Shatursky et al., 1999; Slade et al., 2008). Modeling and labeling of the perforin pore based on a cryo-EM reconstruction indicated, however, an inside-out arrangement of the perforin core relative to the proposed pore model for CDCs (Law et al., 2010). Though a recent crystal structure of the heterotrimeric C8αβγ suggested a CDC-like arrangement of the MAC ring (Lovelace et al., 2011), it lacked the context of the larger MAC assembly. To understand how complement proteins come together to form a lytic pore important for immune defense, we combined crystallographic analysis of C5b6 with electron microscopy (EM) to determine the structure of the sC5b9 complex.

RESULTS

Crystal Structure of C5b6

C5b6 was assembled in vitro, purified, and crystallized. Crystals diffracted anisotropically to a resolution between 3.5 and 4.2 Å, and the structure was solved by molecular replacement (Table S1). The final model, consisting of all 12 domains of C5b and all 10 domains of C6, was refined to a final Rwork/Rfree of 25.6/27.0 and displayed good geometry (Figures 1A–1C, Figure S1A, and Table S1). Because of the limited resolution, we restrict our discussion of the structure to the level of individual domains.

C5 undergoes marked domain rearrangements upon cleavage into C5b and formation of the C5b6 complex. C5 consists of two peptide chains, denoted β (residues [res.] 1–674) and α (res. 678– 1676), that form 13 domains (Fredslund et al., 2008)(Figure 1B). Similar to the conversion of homologous C3 to C3b (Janssen et al., 2006; Janssen et al., 2005), the domains of the α chain undergo major relocations, while most of the β-chain forms a stable ring-like structure (Figure 1E, Table S2, Movie S1). Removal of the anaphylatoxin (ANA/C5a) domain results in extensive movements of the macroglobulin (MG) 3, MG7, MG8, and “complement C1r/C1s, Uegf, Bmp1” (CUB) domains and the thioester-like domain (TED/C5d); C5 lacks the prototypical thioester present in this domain in other members of the C3/

α2-macroglobulin protein family. Although the concerted movement of MG7 and CUB resembles that observed for the C3-C3b transition, the position of the connected TED differs dramatically (Figures 1D and 1E, Table S2). In C5b6, TED is positioned halfway up the β-ring, in contrast to C3b, where TED lies at the "bottom" (Figures 1D and 1E). A requirement for this conformation to be caught and stabilized by C6 may explain the short half-life of the C6 binding site in C5b (Cooper and Müller-Eberhard, 1970). Without C6 binding, C5b will irreversibly decay to a state incapable of binding C6 (Cooper and Müller-Eberhard, 1970).

The structure of C6 in the C5b6 complex reveals that its ten domains can be divided into two functional parts. The first consists of the six N-terminal domains and includes the "core" region common to all MACPF proteins in the MAC; these six domains are thrombospondin (TSP) domain 1, TSP2, low-density lipoprotein receptor class A domain (LDLRa), MACPF, epidermal-growth factor (EGF) domain, and TSP3. The second, C-terminal part consists of two complement-control-protein (CCP) and two factor I/MAC (FIMAC) domains (Figures 1A, 1C, and 1F). These regions are separated by a long flexible linker. A comparison with free C6 (Aleshin et al., 2012) reveals that whereas the N-terminal region is highly similar, the C-terminal region has a strikingly different arrangement (Figures 1A and 1F, Table S3) and forms the major interface with C5b.

The C5b-C6 interface buries ± 3100 $Å^2$ of solvent accessible surface area. The core of C6 binds to the "bottom" of C5b, in between MG1, MG4, and TED, to a highly conserved patch (Figure 2A). A second, major interface is formed by the linker and the CCP1-2 domains of C6 that wrap around the TED domain of C5b (Figure 2A). The CCP1 domain is wedged in between TED, CUB, and MG2 of C5b, where it seems to stabilize the observed position of TED (Figures 1 and 2). The importance of this interaction is supported by data showing that the CCP domains are essential for C6 activity (DiScipio et al., 1999). The linker preceding CCP1 also makes extensive contacts with TED (Figures 2A and 2C), where it interacts in part with a distinct β-hairpin that forms a unique insertion in TED (Figures 2C, 2D and S1B–S1D). We tested the importance of the linker region by mutating several conserved residues, all showing a reduced activity in a hemolytic assay (Figure 2B).

The observed association of C6 to C5b positions the MACPF domain with its putative β-barrel forming transmembrane segments (TMS) at the periphery of the complex (Figure 1A). The two TMS regions in C5b6 (C6 res. 255–312 and res. 381– 438) adopt helical conformations loosely folded onto the central curved four-stranded β sheet of the C6 MACPF; a similar arrangement is observed in structures of free C6 (Aleshin et al., 2012), C8 (Hadders et al., 2007; Lovelace et al., 2011; Slade et al., 2008), perforin (Law et al., 2010), and CDCs (Rossjohn et al., 1997). Importantly, we do not observe a structural rearrangement of these regions compared to free C6, suggesting that binding to C5b is not the trigger for unfolding of these segments. Thus, we interpret the MACPF fold of C6 in C5b6 as a premembrane attack state, which is in agreement with the soluble nature of C5b6.

Cryo-EM of the Soluble Regulated Pore, sC5b9

To understand how the MAC proteins arrange to form a pore, we examined by EM sC5b9 purified from activated serum (Figure S2). Broadly, sC5b9 is a thin, square-shaped complex with a single protrusion at one corner, as suggested by two-dimensional (2D) images (Figure 3, Figures S2A–S2E). Three-dimensional structures of both negatively stained and cryo-EM sC5b9 (Figure S2F) further define two prominent features of the square-like central region. The protrusion (Figure 3A, indicated by a brown arrow) connects to the core at one corner of an arc-shaped crescent, while large connected densities form a butterfly arrangement below the arc (Figure 3A, indicated by a gray surface).

Docking of the C5b6 crystal structure into the 24 Å cryo-EM molecular envelope clearly defined the identity of the protrusion as C5b6. Strikingly, the labile conformation of C5b trapped by C6 in the C5b6 crystal structure is preserved in the larger complex (Figures 1A and 3E). The orientations of the C-terminal FIMAC domains of C6 and the C345C domain of C5b, likely affected by crystal packing, did not fit the density of the sC5b9 reconstruction (Figures S1E–S1G). In addition, the C6 TSP1 domain, thought to regulate assembly of MAC precursors (Aleshin et al., 2012), was also out of density. Our map could accommodate these domains (Figure 3E, indicated by asterisks); however, low resolution precluded modeling their orientations in the sC5b9 reconstruction.

Next, we generated a model of multiple MAC proteins that contain the conserved TSP-LDLRa-MACPF-EGF domain architecture (Figure S3) by duplicating the MACPF-MACPF orientation of C8αβ (Lovelace et al., 2011). Five MAC proteins fit the arc below the protrusion (Figure 3E). Labeling with a monoclonal anti-C9 antibody, recognizing a neo-epitope present in both sC5b9 and the lytic pore, identified C9 as the MAC protein in the arc furthest from the C5b protrusion (Figures 3C–3E and S4). Previous biochemical data showed that C9 binds to C8α (Slade et al., 2006) and that C8β binds C5b7 (Brannen and Sodetz, 2007; Stewart et al., 1987), indicating C8βα as the two MAC components preceding C9. Independent docking of the five-MAC model and C5b6 into the EM map superimposes the core of C6 onto the first MAC position (Figure S3A), suggesting that C6 is the first MAC protein and C7 is in the remaining unoccupied position, the second position between C6 and C8β. Models involving a six-MAC protein arc correlated less well with the EM density (correlation coefficients of 0.88 and 0.84 for five- and six-membered arcs, respectively). It is note-worthy that models involving the C6-C7-C8β-C8α-C9 arrangement, in which the position of C6 was defined by docking C5b6 as a rigid body, correlated 7% better with the map than those ordered C7-C6-C8β-C8α-C9 as previously proposed (Aleshin et al., 2012).

Density in the center of the arc accommodates the lipocalin fold of C8γ (Figure 3E, indicated as a solid gray surface), a MAC component that is flexibly, but covalently, attached to C8α (Lovelace et al., 2011; Slade et al., 2008) (Figure S3C). C8γ enhances lysis, but it is not essential (Parker and Sodetz, 2002) for MAC activity, and its orientation in sC5b9 suggests a role in stabilizing the MACPF-MACPF interactions before closure of the ring. Finally, density present at a ridge along C5b (Figure 3E, indicated with a dashed orange line) could account in part for the unmodeled CCP1-2 and FIMAC1-2 domains of C7, known to interact with the C345C domain of C5b (Thai and Ogata, 2004).

Density of the butterfly-shaped region of the sC5b9 map can be attributed to regulatory proteins, vitronectin and clusterin, known to bind exposed lipophilic regions of MAC precursors. This is supported by previous EM analysis of gold-labeled vitronectin localizing oligomers to this region (Preissner et al., 1989). Moreover, the location of regulatory proteins is consistent with the positioning of predicted transmembrane segments below the MACPFs in the arc and the interpretation that these segments are either disordered or flapped out into their β-hairpin conformation (Figure 4). The structural data, therefore, indicate a potential dual mechanism in protection from pore formation: the two “wings” of the butterfly-shaped regulatory region cap the ends of the MAC arc and thereby block C9 oligomerization, and they enwrap the lipophilic segments to prevent membrane interaction.

DISCUSSION

Pore formation for MACPF-containing proteins involves a dramatic conformational change in which helical bundles transform into a membrane-spanning β-barrel. In contrast to the current model for immune pore formation, which is based on perforin (Law et al., 2010), our

structural analysis of C5b6 and the sC5b9 complex supports a model for the MAC that resembles bacterial CDC pores (Figure 4). Docking of C5b6 into the complex, the curvature of the arc, and density for C8γ inside the pore are all in concordance with the CDC orientation of MACPF proteins in the membrane. Despite its similarity to simpler bacterial pores, the complement-mediated immune response has evolved complex assembly and regulatory mechanisms that are likely required to prevent host tissue damage yet effectively clear pathogen infections. Our model suggests that the ability of C6 to capture a labile binding site in C5b to form an assembly competent state provides the first checkpoint in MAC formation. Next, C7 binds the C5b6 complex, making extensive contacts to C5b through its C-terminal CCP and FIMAC domains, thereby aligning MACPF domains of C6 and C7. Binding of C7 then drives rearrangement of the TMS regions, making C5b7 lipophilic and creating the novel hybrid-binding site for C8. Subsequent association of C8αβγ through alignment of the C8β and C8α MACPF domains relocates C8γ, which in the soluble C8αβγ complex may serve to inhibit C9 association before incorporation into the larger assembly. Finally, host regulatory proteins clusterin and vitronectin can prevent pore formation by blocking both hairpin insertion into the membrane and oligomerisation of C9. Together, our data show how the MAC is assembled and regulated in blood, providing a framework for understanding the role of complement in microbial infection and inflammatory disorders.

EXPERIMENTAL PROCEDURES

Purification of C5b6

C5b6 was isolated from a mixture of purified human C5 and C6 in which the C5 was activated by addition of a mixture of cobra venom factor (CVF), factor B, and factor D in the presence of 0.5 mM $MgCl_2$. C5 and C6 were purified from pooled normal human serum as previously described (Kolb et al., 1982; Tack et al., 1980). The formed C5b6 complex was separated from the other components by ion exchange chromatography over a Mono Q column (GE Healthcare) and subsequently by gel filtration over BioGel A0.5 m (BioRad). Fractions were pooled on the basis of C5b6 functional activity (Rawal and Pangburn, 2000), concentrated to 0.7 mg/ml and dialyzed against 10 mM HEPES (pH 7.2), 120 mM NaCl, and 0.02% w/v NaN_3.

Crystallization and Data Collection

The C5b6 complex was crystallized by vapor diffusion in hanging drops consisting of 2.5 μl protein (0.7 mg/ml) mixed with 0.5 μl 1M HEPES-NaOH (pH 7.8). Drops were equilibrated at 18°C over 300 ml reservoir solution consisting of 0.1M HEPES-NaOH (pH 7.8) and 250 mM NaCl. Crystals grew to maximum dimensions of 800 × 80 × 20 μm in ~3 weeks and were cryoprotected by brief incubation in reservoir solution supplemented with 30% (v/v) ethylene glycol, followed by flash freezing in liquid N_2. A complete data set was collected at ESRF beamline ID29 in seven wedges of 15° that were collected along the length of the crystal through the use of 1° oscillations. The diffraction data were integrated and scaled by XDS (Kabsch, 2010) and Aimless (Collaborative Computational Project, Number 4, 1994). The crystals belong to space group $I2_12_12_1$, have unit-cell parameters of a = 154.2, b = 230.8, and c = 270.0 Å, and contain one complex of C5b6 in the asymmetric unit (solvent content: ~72%). The diffraction data were strongly anisotropic, extending to 4.2 Å resolution in the direction of a*, 3.8 Å in the direction of b*, and 3.5 Å in the direction of c*. These resolution limits were determined by applying a cutoff based on either a mean intensity correlation coefficient of half-data sets > 0.5 or F/σF= 3. Both methods gave the same value for resolution cutoffs.

Structure Determination and Refinement

The structure of C5b6 was solved by molecular replacement through the use of PHASER (McCoy et al., 2007). A solution could be found by using the known structures of C5 (PDB code 3CU7; Fredslund et al., 2008) and C6 (PDB code 3T5O; Aleshin et al., 2012), while prior to the publication of the C6 structure a model of C6 had been generated starting from fragments of homologous structures. The C5 coordinates were separated into TED (res. 986–1305), the β-chain (res. 20–607), and the MG7 (res. 822–931), MG8 (res. 1374–1512), CUB (res. 932–985, 1308–1368), and C345C domains (res. 1530-1676), while the C6 coordinates were separated into the core (res. 22–629), the CCP domains (res. 641–765), and the FIMAC domains (res. 771–934). The model was completed by iterative model building in Coot (Emsley and Cowtan, 2004) and refinement in Phenix (Afonine et al., 2010) and autoBuster (Blanc et al., 2004). Although the data set used for refinement was strongly anisotropic, (4.2–3.5 Å; see above), we used all data up to 3.5 Å for refinement, as anisotropic truncation did not improve refinement statistics or map quality. Initial refinement runs were heavily restrained and involved the use of both secondary structure and Ramachandran restraints as implemented by Phenix (Afonine et al., 2010). In later stages of refinement, the model from Phenix was used to generate LSSR-based target restraints as implemented by autoBuster (Blanc et al., 2004). The refinement strategy further included individual positional and B factor refinement and TLS refinement using 11 TLS groups. The model was refined to an Rfree of 27.0% and displays good geometry, with 88.9% of the residues in the allowed and 0.5% of the residues in the disallowed regions of the Ramachandran plot.

Expression and Purification of C6

C6 constructs were expressed as His6-tagged N-terminal fusions in transiently transfected suspension cultures of N-acetylglucoaminyltransferase-I-deficient HEK293E cells (Utrecht-ProteinExpress). Medium was harvested six days after transfection, then concentrated ~10-fold and buffer-exchanged with the use of a 30 kDa cutoff filter (Quixstand hollow fiber; GE Healthcare). The proteins were purified by Ni-SepharoseTM 6 Fast Flow (GE Healthcare) and size exclusion chromatography with the use of a SuperdexTM 200 10/300 column equilibrated in 20 mM HEPES-NaOH (pH 7.4) and 150 mM NaCl. Fractions containing the C6 construct were pooled, concentrated, and flash frozen in liquid N_2. All proteins were stored at −80°C until use.

Hemolytic Assay

C6 was assayed for hemolytic activity with the use of antibody-sensitized sheep erythrocytes (EA) and C6-depleted human serum (Complement Technology), as described previously (Rawal and Pangburn, 2000). Hemolytic titers (ng C6 required for lyse of 50% of the EA) were determined, and the activities were normalized to recombinant wild-type C6. Each sample was tested at six different concentrations (n = 6). Standard errors were calculated with a nonlinear fitting program (GraFit 5.0, Erithacus software).

Purification of sC5b9

Blood was collected from healthy volunteers and allowed to clot, and serum was separated within 1 hr of collection. To activate complement by both classical and alternative routes, zymosan (10 mg/ml; Sigma) and heat-aggregated human IgG (1mg/ml; made in house) were added to the serum and incubated overnight at 37°C. Particulates were removed by centrifugation and filtration (0.2 μm). Serum was then applied on an affinity column (HiTrap; GE Healthcare) to which 40 mg mouse anti-human C8 monoclonal antibody E2 (generated in house) was coupled. Protein was eluted in 0.1 M glycine (pH 2.5) and neutralized by collection into 0.5 M Tris buffer (pH 8.0). sC5b9 containing fractions were

pooled, concentrated, and applied to a preparative scale gel filtration column (Superdex-200 matrix in a XK16/70 column; GE Healthcare) equilibrated in PBS (137 mM NaCl, 10 mM phosphate, 2.7 mM KCl [pH 7.4]). Immediately before analysis, sC5b9 was further purified by two successive purifications on a Superose 6 PC 3.2/30 gel filtration column in a buffer containing 150 mM NaCl, 50 mM Tris (pH 7.5), 1 mM $CaCl_2$, and 1 mM $MgCl_2$. Antibody-labeled sC5b9 complexes were generated by incubating 5 mgof monoclonal antibody, aE11 (Hycult Biotech), with 7.5 μg sC5b9 for 20 min at room temperature. Excess antibody was removed by gel filtration as described above.

Negative Stain Electron Microscopy

Immediately after gel filtration, a volume of 2.5 μl of sC5b9 (16 μg/ml) or antibody-labeled sC5b-9 (9 μg/ml), were applied to glow-discharged carbon-coated copper grids. Grids were negatively stained with 0.75% uranyl formate. Images were taken under low-dose conditions (~10 $e^-/Å^2$ per exposure) at a nominal magnification of 72,500 on a JEOL JEM-1230 operated at 100 kV. Images were recorded on a 4k × 4k TemCam-F416 camera (TVIPS) and 2.28 Å/pixel. 11330 sC5b9 and 1104 immune-labeled windowed particles were each subjected to reference-free alignment with the use of EMAN2 (Tang et al., 2007) and classified into 149 and 31 classes, respectively. The standard EMAN2 initial-model-generation program (e2initialmodel.py) was used to obtain an initial template for refinement. With the use of this methodology, several models were constructed from a series of randomly generated Gaussian blobs, masked according to the sC5b9 particle diameter, and used to initiate the angular assignment of reference-free-generated 2D class averages. The resulting models were ranked on the basis of the agreement of the projection with the class average. The top choice was used as template for the refinement of negatively stained sC5b9 single particles with the use of EMAN2. Handedness of the map was determined on the basis of an 8% difference in correlation coefficient used for measuring the agreement of the C5b6 crystal structure with the reconstruction.

Cryo-Electron Microscopy

The identical preparation used in the negative stain EM experiments described above was also subjected to analysis by cryo-EM. Aliquots (4 μl) of purified sC5b9 (0.1 mg/ml) were applied to glow-discharged holey carbon grids (QUANTIFOIL R 1.2/1.3) and vitrified in liquid ethane with an FEI Vitrobot. Images were acquired on a JEM-200FS FEG electron microscope (JEOL) operating at 200kV, equipped with an in-column energy filter (OMEGA). Images were recorded with a defocus range of −3.0 to −6.0 microns underfocus and at a magnification of 54,400 on a 4k × 4k ULTRASCAN 4000 SP CCD camera, corresponding to 2.76 Å/pixel. A total of 18,983 individual sC5b9 particles were windowed with e2boxer (EMAN2), corrected for the contrast transfer function (CTF) with Bsoft (Heymann and Belnap, 2007), and low-pass filtered to 11Å. The sC5b9 negative stain reconstruction served as a reference for the refinement of cryo-EM data through the use of projection-matching algorithms in Xmipp (Scheres et al., 2008). All fitting and rigid-body refinement of pseudo-atomic models into the cryo-EM envelope were performed in Chimera (Pettersen et al., 2004). Figures were generated withPymol (PyMOL Molecular Graphics System, version 1.3, Schrödinger).

Supplementary Material

Refer to Web version on PubMed Central for supplementary material.

Acknowledgments

We thank E.Y. Jones for access to computing facilities at University of Oxford, D. Gil for technical support, and S. Rodríguez de Cordoba for advice and discussions. We thank the European Synchrotron Radiation Facility (ESRF) and the Swiss Light Source (SLS) for the provision of synchrotron radiation facilities, and we thank beamline scientists of the SLS, ESRF, and European Molecular Biology Laboratory for assistance. This work was supported by Council for Chemical Sciences of the Netherlands Organization for Scientific Research (NWO-CW) grant 700.57.010, National Institutes of Health (NIH) grant 1 R01 AI072106-01A1; and European Research Council Advanced Grant 233229 to P.G.; Medical Research Council (MRC) grant G0400775 to S.M.L; Wellcome Trust Programme Grant 068590 to B.P.M.; Wellcome Trust Core Award Grant 090532/Z/09/Z; and a grant from the "Ramón Areces" Foundation to O.L. O.L. is also supported by the Spanish Ministry of Science and Innovation (SAF2011-22988), "Red Temática de Investigación Cooperativa en Cáncer (RTICC), Instituto de Salud Carlos III" (RD06/0020/1001), Autonomous Region of Madrid (S2010-BMD-2316), and the Human Frontiers Science Program (RGP39/2008). D.B. is supported by EMBO. M.K.P. is supported by the NIH (grant RO1DK35081).

M.A.H. crystallized C5b6, collected the data, and determined the structure. M.A.H., F.F., and P. R. refined the structure. M.K.P. purified C5b6 and performed hemolytic assays. F.F. purified recombinant C6 mutants. S.H., D.B., and P.R. purified sC5b9. D.B. and O.L. carried out the electron microscopy. D.B. performed the electron microscopy processing and docking analysis. All authors contributed to experimental design, data analysis, and manuscript preparation.

M.K.P. is an officer of and has a financial interest in Complement Technology, Inc., a supplier of complement reagents.

REFERENCES

Afonine PV, Mustyakimov M, Grosse-Kunstleve RW, Moriarty NW, Langan P, Adams PD. Joint X-ray and neutron refinement with phenix.refine. Acta Crystallogr. D Biol. Crystallogr. 2010; 66:1153–1163. [PubMed: 21041930]

Aleshin AE, Schraufstatter IU, Stec B, Bankston LA, Liddington RC, Discipio RG. Structure of Complement C6 suggests a mechanism for initiation and unidirectional, sequential assembly of the Membrane Attack Complex (MAC). J. Biol. Chem. 2012

Bhakdi S, Bhakdi-Lehnen B, Tranum-Jensen J. Proteolytic transformation of SC5b-9 into an amphiphilic macromolecule resembling the C5b-9 membrane attack complex of complement. Immunology. 1979; 37:901–912. [PubMed: 115783]

Blanc E, Roversi P, Vonrhein C, Flensburg C, Lea SM, Bricogne G. Refinement of severely incomplete structures with maximum likelihood in BUSTER-TNT. Acta Crystallogr. D Biol. Crystallogr. 2004; 60:2210–2221. [PubMed: 15572774]

Botto M, Kirschfink M, Macor P, Pickering MC, Würzner R, Tedesco F. Complement in human diseases: Lessons from complement deficiencies. Mol. Immunol. 2009; 46:2774–2783. [PubMed: 19481265]

Brannen CL, Sodetz JM. Incorporation of human complement C8 into the membrane attack complex is mediated by a binding site located within the C8beta MACPF domain. Mol. Immunol. 2007; 44:960–965. [PubMed: 16624411]

Collaborative Computational Project, Number 4. The CCP4 suite: programs for protein crystallography. Acta Crystallogr. D Biol. Crystallogr. 1994; 50:760–763. [PubMed: 15299374]

Cooper NR, Müller-Eberhard HJ. The reaction mechanism of human C5 in immune hemolysis. J. Exp. Med. 1970; 132:775–793. [PubMed: 5508377]

DiScipio RG, Linton SM, Rushmere NK. Function of the factor I modules (FIMS) of human complement component C6. J. Biol. Chem. 1999; 274:31811–31818. [PubMed: 10542204]

Emsley P, Cowtan K. Coot: model-building tools for molecular graphics. Acta Crystallogr. D Biol. Crystallogr. 2004; 60:2126–2132. [PubMed: 15572765]

Esser AF. The membrane attack complex of complement. Assembly, structure and cytotoxic activity. Toxicology. 1994; 87:229–247. [PubMed: 8160186]

Fredslund F, Laursen NS, Roversi P, Jenner L, Oliveira CLP, Pedersen JS, Nunn MA, Lea SM, Discipio R, Sottrup-Jensen L, Andersen GR. Structure of and influence of a tick complement inhibitor on human complement component 5. Nat. Immunol. 2008; 9:753–760. [PubMed: 18536718]

Hadders MA, Beringer DX, Gros P. Structure of C8alpha-MACPF reveals mechanism of membrane attack in complement immune defense. Science. 2007; 317:1552–1554. [PubMed: 17872444]

Heymann JB, Belnap DM. Bsoft: image processing and molecular modeling for electron microscopy. J. Struct. Biol. 2007; 157:3–18. [PubMed: 17011211]

Janssen BJ, Huizinga EG, Raaijmakers HC, Roos A, Daha MR, Nilsson-Ekdahl K, Nilsson B, Gros P. Structures of complement component C3 provide insights into the function and evolution of immunity. Nature. 2005; 437:505–511. [PubMed: 16177781]

Janssen BJ, Christodoulidou A, McCarthy A, Lambris JD, Gros P. Structure of C3b reveals conformational changes that underlie complement activity. Nature. 2006; 444:213–216. [PubMed: 17051160]

Kabsch W. Xds. Acta Crystallogr. D Biol. Crystallogr. 2010; 66:125–132. [PubMed: 20124692]

Kolb WP, Kolb LM, Savary JR. Biochemical characterization of the sixth component (C6) of human complement. Biochemistry. 1982; 21:294–301. [PubMed: 7074016]

Law RH, Lukoyanova N, Voskoboinik I, Caradoc-Davies TT, Baran K, Dunstone MA, D'Angelo ME, Orlova EV, Coulibaly F, Verschoor S, et al. The structural basis for membrane binding and pore formation by lymphocyte perforin. Nature. 2010; 468:447–451. [PubMed: 21037563]

Lovelace LL, Cooper CL, Sodetz JM, Lebioda L. Structure of human C8 protein provides mechanistic insight into membrane pore formation by complement. J. Biol. Chem. 2011; 286:17585–17592. [PubMed: 21454577]

McCoy AJ, Grosse-Kunstleve RW, Adams PD, Winn MD, Storoni LC, Read RJ. Phaser crystallographic software. J. Appl. Cryst. 2007; 40:658–674. [PubMed: 19461840]

Mollnes TE, Lea T, Harboe M, Tschopp J. Monoclonal antibodies recognizing a neoantigen of poly(C9) detect the human terminal complement complex in tissue and plasma. Scand. J. Immunol. 1985; 22:183–195. [PubMed: 4035298]

Morgan BP. Regulation of the complement membrane attack pathway. Crit. Rev. Immunol. 1999; 19:173–198. [PubMed: 10422598]

Parker CL, Sodetz JM. Role of the human C8 subunits in complement-mediated bacterial killing: evidence that C8 gamma is not essential. Mol. Immunol. 2002; 39:453–458. [PubMed: 12413696]

Pettersen EF, Goddard TD, Huang CC, Couch GS, Greenblatt DM, Meng EC, Ferrin TE. UCSF Chimera—a visualization system for exploratory research and analysis. J. Comput. Chem. 2004; 25:1605–1612. [PubMed: 15264254]

Podack ER, Müller-Eberhard HJ. SC5b-9 complex of complement: formation of the dimeric membrane attack complex by removal of S-protein. J. Immunol. 1980; 124:1779–1783. [PubMed: 6988507]

Podack ER, Tschoop J, Müller-Eberhard HJ. Molecular organization of C9 within the membrane attack complex of complement. Induction of circular C9 polymerization by the C5b-8 assembly. J. Exp. Med. 1982; 156:268–282. [PubMed: 6177822]

Preissner KT, Podack ER, Müller-Eberhard HJ. The membrane attack complex of complement: relation of C7 to the metastable membrane binding site of the intermediate complex C5b-7. J. Immunol. 1985; 135:445–451. [PubMed: 3998468]

Preissner KP, Podack ER, Müller-Eberhard HJ. SC5b-7, SC5b-8 and SC5b-9 complexes of complement: ultrastructure and localization of the S-protein (vitronectin) within the macromolecules. Eur. J. Immunol. 1989; 19:69–75. [PubMed: 2465906]

Rawal N, Pangburn MK. Functional role of the noncatalytic subunit of complement C5 convertase. J. Immunol. 2000; 164:1379–1385. [PubMed: 10640753]

Rosado CJ, Buckle AM, Law RH, Butcher RE, Kan WT, Bird CH, Ung K, Browne KA, Baran K, Bashtannyk-Puhalovich TA, et al. A common fold mediates vertebrate defense and bacterial attack. Science. 2007; 317:1548–1551. [PubMed: 17717151]

Rossjohn J, Feil SC, McKinstry WJ, Tweten RK, Parker MW. Structure of a cholesterol-binding, thiol-activated cytolysin and a model of its membrane form. Cell. 1997; 89:685–692. [PubMed: 9182756]

Scheres SH, Núñez-Ramírez R, Sorzano CO, Carazo JM, Marabini R. Image processing for electron microscopy single-particle analysis using XMIPP. Nat. Protoc. 2008; 3:977–990. [PubMed: 18536645]

Shatursky O, Heuck AP, Shepard LA, Rossjohn J, Parker MW, Johnson AE, Tweten RK. The mechanism of membrane insertion for a cholesterol-dependent cytolysin: a novel paradigm for pore-forming toxins. Cell. 1999; 99:293–299. [PubMed: 10555145]

Slade DJ, Chiswell B, Sodetz JM. Functional studies of the MACPF domain of human complement protein C8alpha reveal sites for simultaneous binding of C8beta, C8gamma, and C9. Biochemistry. 2006; 45:5290–5296. [PubMed: 16618117]

Slade DJ, Lovelace LL, Chruszcz M, Minor W, Lebioda L, Sodetz JM. Crystal structure of the MACPF domain of human complement protein C8 alpha in complex with the C8 gamma subunit. J. Mol. Biol. 2008; 379:331–342. [PubMed: 18440555]

Steckel EW, Welbaum BE, Sodetz JM. Evidence of direct insertion of terminal complement proteins into cell membrane bilayers during cytolysis. Labeling by a photosensitive membrane probe reveals a major role for the eighth and ninth components. J. Biol. Chem. 1983; 258:4318–4324. [PubMed: 6833260]

Stewart JL, Kolb WP, Sodetz JM. Evidence that C5b recognizes and mediates C8 incorporation into the cytolytic complex of complement. J. Immunol. 1987; 139:1960–1964. [PubMed: 3624872]

Tack BF, Harrison RA, Janatova J, Thomas ML, Prahl JW. Evidence for presence of an internal thiolester bond in third component of human complement. Proc. Natl. Acad. Sci. USA. 1980; 77:5764–5768. [PubMed: 6934510]

Tang G, Peng L, Baldwin PR, Mann DS, Jiang W, Rees I, Ludtke SJ. EMAN2: an extensible image processing suite for electron microscopy. J. Struct. Biol. 2007; 157:38–46. [PubMed: 16859925]

Thai CT, Ogata RT. Complement components C5 and C7: recombinant factor I modules of C7 bind to the C345C domain of C5. J. Immunol. 2004; 173:4547–4552. [PubMed: 15383587]

Tschopp J. Ultrastructure of the membrane attack complex of complement. Heterogeneity of the complex caused by different degree of C9 polymerization. J. Biol. Chem. 1984; 259:7857–7863. [PubMed: 6736027]

Tschopp J, Podack ER, Müller-Eberhard HJ. The membrane attack complex of complement: C5b-8 complex as accelerator of C9 polymerization. J. Immunol. 1985; 134:495–499. [PubMed: 3964819]

Europe PMC Funders Author Manuscripts

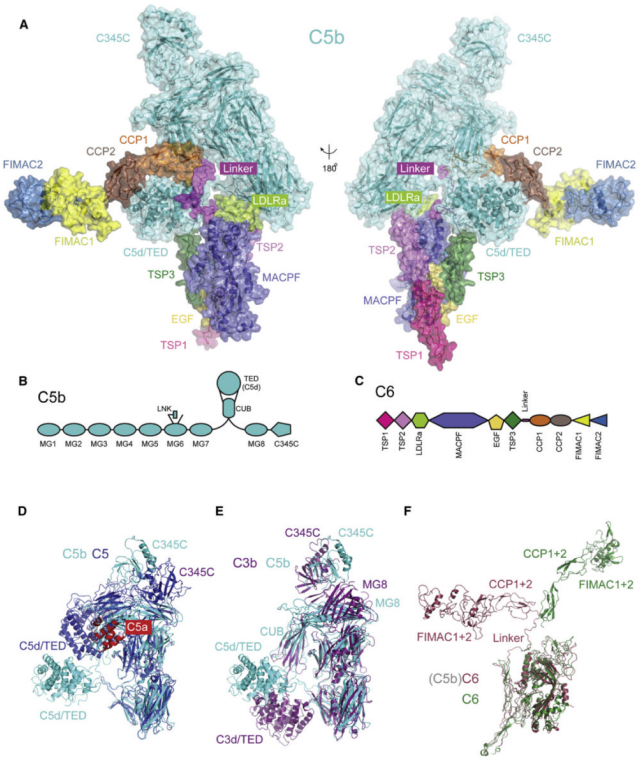

Figure 1. The Structure of C5b6

(A) A cartoon and surface representation of C5b6 in two orientations. C5b is colored in cyan, and C6 is colored by domain boundaries.

(B) A schematic representation of the domain architecture of C5b.

(C) A schematic representation of the domain architecture of C6.

(D) A cartoon representation of C5b (cyan) superimposed onto C5 (blue; PDB code 3CU7). C5a is colored red.

(E) A cartoon representation of C5b (cyan) superimposed onto C3b (purple; PDB code 2I07).

(F) A cartoon representation of C6 from the C5b-C6 complex (brown) superimposed onto free C6 (green; PDB code 3T5O), based on their MACPF domains.

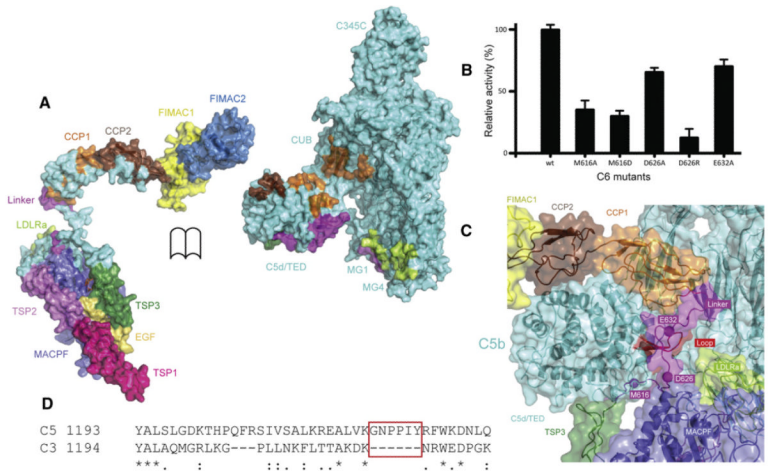

Figure 2. Interface of the C5b6 Complex

(A) The interface between C5b and C6 with the complex “spread” apart. C5b is cyan, with the C6 footprint colored according to the contacting C6 domains. C6 is colored as in Figure 1, and the footprint of C5b is cyan.

(B) Hemolytic activity of C6 linker mutants expressed as a percentage relative to recombinant wild-type C6. Each sample was tested at six different concen trations, and standard errors were determined with the use of a nonlinear fitting program (GraFit 5.0).

(C) A close-up of the C5b-C6 interaction shows the extensive interface between TED and the C6 linker. Mutated residues tested in (B) are shown as spheres. The unique β-hairpin of C5 (TED) that interacts with the linker is highlighted in red.

(D) Structure-based alignment of C5 and C3; the unique insertion in C5 is boxed.

Europe PMC Funders Author Manuscripts

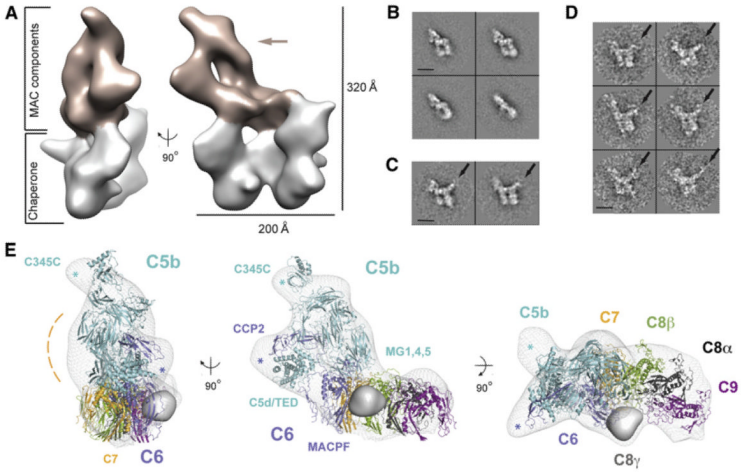

Figure 3. Cryo-EM Structure of sC5b9

(A) MAC components (brown surface) consist of an arc-shaped crescent with a single protrusion (brown arrow), while regulatory domains form a butterfly-like structure (gray surface) below.

(B) Class averages of negatively stained sC5b9.

(C) Additional density present in the antiC9:sC5b9 averages identifies C9 in the complex (black arrow).

(D) Raw images of antiC9:sC5b9. Black arrow indicates antibody.

(E) Pseudoatomic model for MAC components consists of C5b6 (C5b, cyan; C6, blue), and C8 (C8α, dark gray; C8β, green; C8γ, light gray solid surface) crystal structures and models for C7 (orange) and C9 (purple). The dashed orange line indicates a ridge connecting the arc with C345C. Cyan and blue asterisks indicate unmodeled density near C345C of C5b and CCP1 of C6, respectively.

Scale bars represent 160 Å (B–D).

Europe PMC Funders Author Manuscripts

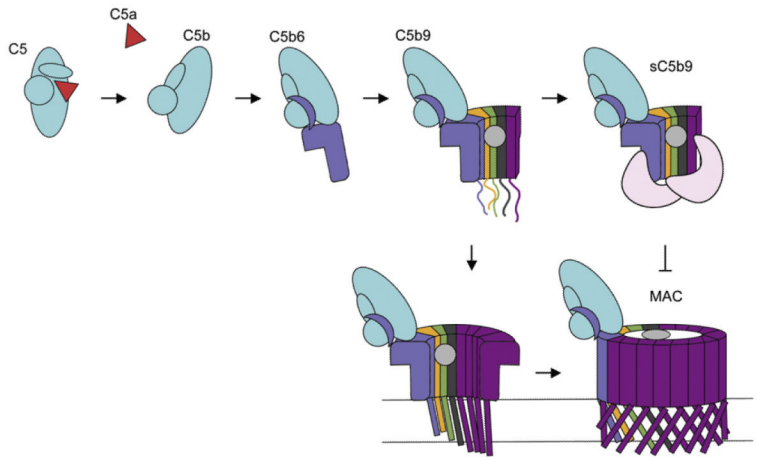

Figure 4. A Model for MAC Formation

The complement terminal pathway is initiated by the cleavage of C5 to C5b. C6 traps a labile conformation of the C5b TED domain to form C5b6, a platform for the stepwise assembly of components C7, C8, and C9. Regulatory proteins in the plasma block MAC assembly in solution by binding exposed hydrophobic regions and sterically inhibit C9 oligomerization. Binding of C5b8 to membranes recruits multiple C9 molecules whose MACPF domains arrange to form a β-barrel pore similar to that of CDCs.